1521-0111/105/3/213–223$35.00
MOLECULAR PHARMACOLOGY

dx.doi.org/10.1124/molpharm.123.000784
Mol Pharmacol 105:213–223, March 2024

Extrahelical Binding Site for a 1*H*-Imidazo[4,5-c]quinolin-4-amine A_3 Adenosine Receptor Positive Allosteric Modulator on Helix 8 and Distal Portions of Transmembrane Domains 1 and 7[S]

Courtney L. Fisher, Matteo Pavan, Veronica Salmaso, Robert F. Keyes, Tina C. Wan, Balaram Pradhan, Zhan-Guo Gao, Brian C. Smith, Kenneth A. Jacobson, and John A. Auchampach

Departments of Pharmacology & Toxicology and the Cardiovascular Center (C.L.F., T.C.W., J.A.A.) and Biochemistry and the Program in Chemical Biology (R.F.K., B.C.S.), Medical College of Wisconsin, Milwaukee, Wisconsin; Molecular Recognition Section, Laboratory of Bioorganic Chemistry, National Institute of Diabetes and Digestive and Kidney Diseases, National Institutes of Health, Bethesda, Maryland (M.P., V.S., B.P., Z.-G.G., K.A.J.); and Department of Pharmaceutical and Pharmacological Sciences, University of Padua, Padua, Italy (V.S.)

Received August 16, 2023; accepted December 12, 2023

ABSTRACT

This study describes the localization and computational prediction of a binding site for the A_3 adenosine receptor (A_3AR) positive allosteric modulator 2-cyclohexyl-1*H*-imidazo[4,5-c]quinolin-4-(3,4-dichlorophenyl)amine (LUF6000). The work reveals an extrahelical lipid-facing binding pocket disparate from the orthosteric binding site that encompasses transmembrane domain (TMD) 1, TMD7, and Helix (H) 8, which was predicted by molecular modeling and validated by mutagenesis. According to the model, the nearly planar 1*H*-imidazo[4,5-c]quinolinamine ring system lies parallel to the transmembrane segments, inserted into an aromatic cage formed by π-π stacking interactions with the side chains of $Y284^{7.55}$ in TMD7 and $Y293^{8.54}$ in H8 and by π-NH bonding between $Y284^{7.55}$ and the exocyclic amine. The 2-cyclohexyl group is positioned "upward" within a small hydrophobic subpocket created by residues in TMDs 1 and 7, while the 3,4-dichlorophenyl group extends toward the lipid interface. An H-bond between the N-1 amine of the heterocycle and the carbonyl of $G29^{1.49}$ further stabilizes the interaction. Molecular dynamics simulations predicted two metastable intermediates, one resembling a pose determined by molecular docking and a second involving transient interactions with $Y293^{8.54}$; in simulations, each of these intermediates converges into the final bound state. Structure-activity-relationships for replacement of either of the identified exocyclic or endocyclic amines with heteroatoms lacking H-bond donating ability were consistent with the hypothetical pose. Thus, we characterized an allosteric pocket for 1*H*-imidazo[4,5-c]quinolin-4-amines that is consistent with data generated by orthogonal methods, which will aid in the rational design of improved A_3AR positive allosteric modulators.

SIGNIFICANCE STATEMENT

Orthosteric A_3AR agonists have advanced in clinical trials for inflammatory conditions, liver diseases, and cancer. Thus, the clinical appeal of selective receptor activation could extend to allosteric enhancers, which would induce site- and time-specific activation in the affected tissue. By identifying the allosteric site for known positive allosteric modulators, structure-based drug discovery modalities can be enabled to enhance the pharmacological properties of the 1*H*-imidazo[4,5-c]quinolin-4-amine class of A_3AR positive allosteric modulators.

Introduction

Pharmaceutical targeting of the A_3 adenosine receptor (A_3AR) has emerged as a promising therapeutic approach for a broad spectrum of diseases that are driven by chronic inflammation. The A_3AR is a G_i protein-coupled receptor that is abundantly expressed in various immune cell populations including granulocytic cells (neutrophils, eosinophils, basophils, mast cells), macrophages, and microglia, where it controls chemotaxis and cellular activation (Walker et al., 1997; Jordan et al., 1999; Hammarberg et al., 2003; Chen et al., 2006; Haskó et al., 2008;

This research was supported in part by National Institutes of Health National Heart, Lung, and Blood Institute [Grant R01 HL133589] (to J.A.A.), National Institutes of General Medicine Sciences [Grant R35 GM128840] (to B.C.S.), National Heart, Lung, and Blood Institute [Grant F31 HL160193] (to C.L.F.), the National Institute of Diabetes and Digestive and Kidney Diseases Intramural Research Program [Grant ZIADK031117] (to K.A.J.), the American Heart Association (Predoctoral Fellowship) [Grant 898217] (to C.L.F.), and the Medical College of Wisconsin Therapeutic Accelerator Program (to J.A.A.).

No author has an actual or perceived conflict of interest with the contents of this article.

dx.doi.org/10.1124/molpharm.123.000784.

[S] This article has supplemental material available at molpharm.aspetjournals.org.

ABBREVIATIONS: A_3AR, A_3 adenosine receptor; AB-MECA, N^6-4-aminobenzyl)adenosine-5′-*N*-methylcarboxamide; Cl-IB-MECA, 2-chloro-N^6-(3-iodobenzyl)adenosine-5′-*N*-methylcarboxamide; GPCR, G protein-coupled receptor; H, Helix; HEK293, human embryonic kidney 293; [^{125}I]I-AB-MECA, N^6-(4-amino-3-[^{125}I]iodobenzyl)adenosine-5′-*N*-methylcarboxamide; IB-MECA, N^6-(3-iodobenzyl)adenosine-5′-*N*-methylcarboxamide; LUF6000, 2-cyclohexyl-1*H*-imidazo[4,5-c]quinolin-4-(3,4-dichlorophenyl)amine; OS9, orphan site 9PAM, positive allosteric modulator; RMSD, root mean square deviation; [^{35}S]GTPγS, guanosine 5′-[γ-[^{35}S]thio]triphosphate; TMD, transmembrane domain.

van der Hoeven et al., 2008; Ge et al., 2010; van der Hoeven et al., 2010; Antonioli et al., 2022; Gao et al., 2023). Moderately selective nucleoside agonists for the A_3AR first developed nearly 30 years ago, including N^6-(3-iodobenzyl)adenosine-5′-*N*-methylcarboxamide (IB-MECA) and its 2-chloro derivative Cl-IB-MECA, are currently in advanced clinical trials for the treatment of psoriasis, nonalcoholic steatohepatitis, and hepatocellular carcinoma (Fishman et al., 2023). Newer nucleoside agonists containing a rigid ribose substitution, some of which are greater than 10,000-fold selective verses the other adenosine receptor subtypes (A_1, A_{2A}, and A_{2B}ARs), are being developed for the treatment of neuropathic pain, stroke, and traumatic brain injury (Liston et al., 2020, 2022; Bozdemir et al., 2021).

As an alternative and more precise approach to target the A_3 AR, we have pursued the development of positive allosteric modulators (PAMs) for the clinically important A_3AR. G protein-coupled receptor (GPCR) PAMs are ligands that act at an allosteric site outside the orthosteric binding site for the endogenous agonist, thereby magnifying signaling by increasing orthosteric agonist binding affinity resulting in an increase in potency and/or by increasing the orthosteric agonist signaling efficacy (Coughlin et al., 2019; Slosky et al., 2021; Wang et al., 2021). The advantages of allosteric modulators include the potential for greater specificity since allosteric sites are not subjected to evolutionary pressures to accommodate a shared ligand across receptor subtypes. The spatiotemporal specificity of PAMs, in principle, reduces the risk of unwanted, on-target side effects and the potential for efficacy loss due to receptor desensitization.

In prior work, we have developed an A_3AR PAM, named LUF6000, and its congeners based on the 1*H*-imidazo[4,5-c]quinolin-4-amine chemical scaffold (Fig. 1) (Gao et al., 2002, 2008, 2011; Göblyös et al., 2006; Kim et al., 2009; Du et al., 2012, 2018; Fallot et al., 2022; Fisher et al., 2022). LUF6000 displays positive cooperativity with orthosteric agonists, enhancing their A_3AR binding and potentiating agonist-induced downstream signaling. Uniquely, LUF6000 has been shown in transfected human embryonic kidney 293 (HEK293) cells to selectively enhance signaling by specific Gα protein isoforms ($G\alpha_{i3}$ and $G\alpha_{0A}$) without potentiating β-arrestin2 recruitment. This suggests that LUF6000 and its congeners may bias signaling in cells that coexpress the A_3AR and specific Gα protein isoforms, such as spinal cord neurons involved in pain sensation and immune cells (Fisher et al., 2022). Unfortunately, at higher concentrations approaching 1 to 10 μM, essentially all of the 1*H*-imidazo[4,5-c]quinolin-4-amine derivatives thus far synthesized and characterized begin to reduce agonist potency due to a mechanism of action involving direct competition for orthosteric site binding. Another disadvantage of LUF6000 and all other similar 1*H*-imidazo[4,5-c]quinolin-4-amine derivatives we have investigated to date is that they are only weakly active at rodent A_3ARs, thereby limiting the ability to test for efficacy in experimental animal models of disease (Du et al., 2018; Fallot et al., 2022; Fisher et al., 2022). Thus, we continue to search for improved derivatives with rodent activity and less propensity to reduce agonist potency; to date this endeavor is impeded by the lack of A_3AR structural information to help guide drug design decisions.

Due to rapid advances in structural and computational biology, the diversity of allosteric binding sites for GPCRs is becoming increasingly appreciated. Locations of PAM binding sites that have been verified include the "extracellular vestibule" of muscarinic receptors comprising the extracellular face of the transmembrane domain (TMD) bundle that lines the path leading to the orthosteric site deeper within the transmembrane core (Burger et al., 2018; Nguyen et al., 2022; van der Westhuizen et al., 2021). However, a β_2 adrenergic receptor PAM (Compound-6A) and a dopamine D_1 receptor PAM (DETQ) each bind on their respective receptor's inner surface in a pocket created by intracellular loop 2 and TMDs 3 and 4 (Wang et al., 2018; Liu et al., 2019). More recently, a cryogenic electron microscopic structure of the A_1 adenosine receptor, complexed with adenosine, the αi_2 G protein subunit, and the PAM MIPS521 was reported (Draper-Joyce et al., 2021). Here, MIPS521 was described to bind to an intramembrane extrahelical site that involves TMDs 1, 6, and 7. With each of these uniquely positioned, diverse sites, allosteric ligand binding is hypothesized to alter the receptor's ability to transition between active and inactive states, providing positive cooperativity.

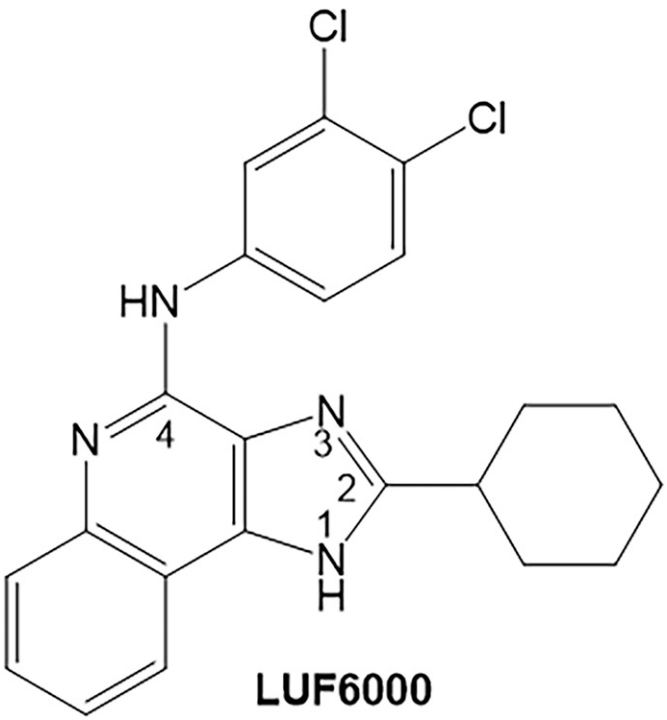

Fig. 1. Chemical structure of the 1*H*-imidazo[4,5-c]quinoline-4-amine A_3AR positive allosteric modulator LUF6000.

Previously, we exploited species differences using a human (responding species)/mouse (nonresponding species) chimeric receptor approach to localize the LUF6000 binding pocket to the inner portions (with respect to the lipid bilayer) of the receptor (Fisher et al., 2022). In the current study, the binding region was narrowed further, informed by additional chimeric receptor studies, which was followed by induced-fit docking and molecular dynamics to pinpoint the binding site for LUF6000. This site is located in an extrahelical, lipid-facing pocket formed outside the receptor core similar to that described for the A_1AR, except in this case binding interactions occur with TMD1, TMD7, and Helix (H)8.

Materials and Methods

Materials. Unless noted otherwise, all chemicals and reagents were purchased from Sigma-Aldrich (St. Louis, MO). Mycoplasma-free

HEK293 cells were purchased from the American Type Tissue Collection (#CRL-1573, Manassas, VA). The cells were further tested for possibility of mycoplasm contamination on a yearly basis. Cell culture media and additional components were from Thermo Fisher (Waltham, MA). LUF6000 was custom synthesized as previously described at a purity of > 95% (Göblyös et al., 2006).

Creation of HEK293 Cells Lines Expressing Adenosine Receptors. Full-length cDNAs encoding wild-type human (AY136749.1), wild-type mouse (NM_009631.4), human/mouse chimeric, and mutated A_3 ARs were synthesized commercially (Top Gene Technologies, St. Laurent, Quebec) and subcloned into pcDNA3.1 (#V79020, Invitrogen, Carlsbad, CA). Plasmids were transfected into HEK293 cells using TransIT-293 transfection reagent (#MIR 2704, Mirus Bio, Madison, WI) and selected using 2 mg/ml G418 (#G-418-5, Goldbio, St. Louis, MO) in cell culture media (DMEM with 10% fetal bovine serum, 100 units/ml penicillin, and 100 mg/ml streptomycin). Cell lines derived from individual clones were maintained in media containing 0.6 mg/ml G418. The expression level of each cell line expressing mutant receptors was similar (~1,000–3,000 fmol/mg protein) based on saturation radioligand binding analysis (Supplemental Table 1).

Membrane Preparations. HEK293 cells were washed with PBS followed by homogenization in Buffer A containing 10 mM Na-HEPES (pH 7.4), 10 mM EDTA, and 1 mM benzamidine and centrifuged (27,000 × g) for 30 min at 4°C. Cell pellets were rehomogenized in Buffer A (except the EDTA concentration was reduced to 1 mM) and centrifuged. The supernatant was discarded, and cell pellets were resuspended in Buffer A (1 mM EDTA) containing 10% glucose and stored at -20°C.

Guanosine 5′-[γ-[^{35}S]thio]triphosphate Binding Assays. HEK293 cell membranes (5–10 μg of protein) were pretreated with LUF6000 for 1 h in 100 μl of GTPγS binding buffer (50 mM Tris HCl at pH 7.4, 1 mM EGTA, 10 mM $MgCl_2$, 100 mM NaCl, 0.004% 3-[(3-cholamidopropyl)dimethylammonio]-1-propanesulfonic acid, and 0.5% bovine serum albumin) in a 96-well, large-volume polypropylene plate (Du et al., 2018; Fisher et al., 2022). In all assays, ZM241385 and PSB-603 (#1026 and 3198, respectively, Tocris, Bristol, UK), each at a final concentration of 300 nM, were included in the assays to block A_{2B} expressed endogenously in HEK293 cells. Adenosine deaminase (1 unit/ml; #10102105001, Roche Diagnostics, Mannheim, Germany) was also included to degrade adenosine present in the assay. The reactions were initiated by the addition of ~0.2 nM guanosine 5′-[γ-[^{35}S]thio]triphosphate ([^{35}S]GTPγS) (#NEG030H250UC, Perkin-Elmer, Waltham, MA) and the selective A_3AR agonist Cl-IB-MECA (#1104, Tocris, Bristol, UK) at the indicated concentrations, performed in triplicate, and incubated for 2 h at room temperature. At the end of the 2-h incubation period, the membranes were harvested by rapid filtration through Whatman GF/B filters (#FP-105, Brandel, Gaithersburg, MD) presoaked in GTPγS binding buffer containing 0.02% 3-[(3-cholamidopropyl)dimethylammonio]-1-propanesulfonic acid using a 96-well cell harvester (Brandel). Radioactivity trapped by the filter was measured by scintillation counting. Nonspecific binding was determined in the presence of 10 μM unlabeled GTPγS (#G8634, Sigma-Aldrich). Results with LUF6000 are normalized to the E_{max} value obtained in the presence of the vehicle.

[^{125}I]I-AB-MECA Binding Assays. Cell membranes (50 μg) were incubated in 100 μl of binding buffer (50 mM Tris-HCl at pH 7.4, 10 mM $MgCl_2$, 1 mM EDTA, and 1 unit/ml adenosine deaminase) containing ~0.3 nM [^{125}I]N^6-(4-amino-3-iodobenzyl)-adenosine-5′-*N*-methylcarboxamide ([^{125}I]I-AB-MECA) (Melman et al., 2008; Paoletta et al., 2013). The reactions, performed in triplicate, were incubated at room temperature for the times indicated, after which bound and free radioligand were separated by rapid filtration through GF/C glass fiber filters (#FP-205, Brandel). Radioactivity trapped by the filters was measured using a gamma counter. For dissociation studies, [^{125}I]I-AB-MECA was incubated with membranes for 3 h to achieve equilibrium, after which the assays were initiated by the addition of adenosine-5′-*N*-ethylcarboxamide (100 μM; #1691, Tocris, Bristol, UK), along with LUF6000 (10 μM) or equivalent vehicle (DMSO). Specific [^{125}I]I-AB-MECA binding was measured by rapid filtration at the indicated times. Nonspecific binding was measured by including 100 μM adenosine-5′-N-ethylcarboxamide for the duration of the assay. For equilibrium binding assays, membranes were incubated for 3 h with 6 to 8 concentrations of [^{125}I]I-AB-MECA for 3 h before filtration; the specific activity of [^{125}I]I-AB-MECA was reduced 10- to 20-fold with the nonradioactive compound. [^{125}I]I-AB-MECA (specific activity ~2,200 Ci/mmol) was prepared by radioiodination of AB-MECA (#28415, Cayman Chemical, Ann Arbor, MI) using the chloramine-T method and purified by high-pressure liquid chromatography (Auchampach et al., 1997).

Molecular Modeling. Detailed procedures for A_3AR protein structure prediction, molecular docking, and molecular dynamics are described in detail in the Supplemental Material file.

Data Analysis. For [^{35}S]GTPγS binding assays, EC_{50} and E_{max} values were calculated from data obtained from concentration-response curves according to: $E = (E_{Max} * x)/(EC_{50} + x)$, in which x is the concentration of Cl-IB-MECA. For [^{125}I]I-AB-MECA dissociation binding assays, data were fit to a one-phase exponential decay model: $Y = (Y_0 - NS)e^{(-k * t)}$, in which Y_0 is specific binding at time 0, *k* is the dissociation rate constant, NS is nonspecific binding, and t is elapsed time. Data (K_d and B_{max} values) from [^{125}I]I-AB-MECA saturation binding assays were fit optimally to a one-site binding model described within the GraphPad (version 9.5.1) package that accounts for ligand depletion to determine K_d and B_{max} values. All values are presented as the mean ± S.D. Data were compared using unpaired Student's *t* tests or one-way ANOVA with Dunnett's multiple comparison tests to identify concentrations of LUF6000 that produced changes in the EC_{50} and/or E_{max} of Cl-IB-MECA compared with vehicle (DMSO). A P value < 0.05 was considered statistically significant. Please note that this study was exploratory and not designed to test a prespecified null hypothesis. Therefore, calculated P values are descriptive only and must not be interpreted as hypothesis testing.

Results

A_3AR Human/Mouse Chimeras

Our recently published work with human/mouse chimeras predicted the allosteric binding pocket for LUF6000 to be within the lower portions of the A_3AR but did not delineate which of the TMDs and their corresponding intracellular loops is/are involved (Fisher et al., 2022). Therefore, we generated four new chimeric receptors depicted in Figs. 2 and 3A, in which we replaced the human A_3AR sequence with the mouse sequence. The first three chimeras replaced each individual intracellular loop along with the lower half of each connecting TMD on either side with the mouse sequence, which were designated $H/M_{TMD1\text{-}2/ICL1}$, $H/M_{TMD3\text{-}4/ICL2}$, and $H/M_{TMD5\text{-}6/ICL3}$. Separation between proximal and distal portions of the TMDs was ×.50 per the Ballesteros–Weinstein numbering system, where amino acid ×.50 is the most conserved amino acid within that TMD (Ballesteros and Weinstein, 1995). The fourth chimera ($H/M_{TMD7/H8/CT}$) replaced the distal portion of TMD7, H8, and the C-terminus with the mouse sequence. Residue C303$^{8.64}$ within H8 is a palmitoylation site and defines the border between H8 and the C-terminal tail. As shown in Fig. 2, the number of amino acid differences for each chimera were as follows: $H/M_{TMD1\text{-}2/ICL1} = 4$, $H/M_{TMD3\text{-}4/ICL2} = 2$, $H/M_{TMD5\text{-}6/ICL3} = 9$, and $H/M_{TMD7/H8/CT} = 1$ in TMD7, 4 in H8, and 8 in the C-terminus (13 total).

Each chimera was evaluated in [^{35}S]GTPγS binding assays to assess G protein exchange activity. Concentration-response curves were performed with the A_3AR-selective orthosteric agonist Cl-IB-MECA (10^{-11}–10^{-5} M) in the presence of either vehicle (DMSO) or 0.1, 1, or 10 μM LUF6000. For each chimera,

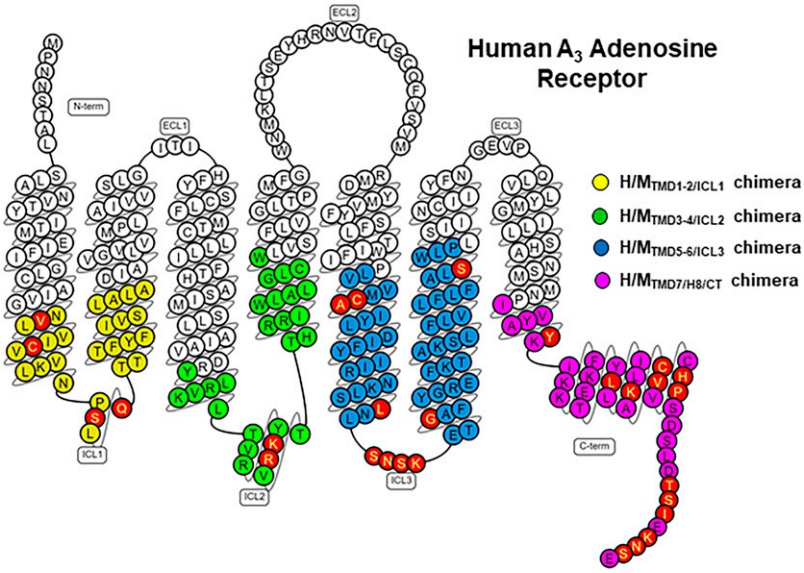

Fig. 2. Strategy for creating human/mouse chimeric receptors. (A) Snake diagram of the human A_3AR amino acid sequence. Colored circles demarcate regions that were scanned for differences between the human and mouse sequences for the following chimeras: yellow = H/$M_{TMD1\text{-}2/ICL1}$, green = H/$M_{TMD3\text{-}4/ICL2}$, blue = H/$M_{TMD5\text{-}6/ICL3}$, purple = H/$M_{TMD7/H8/CT}$. Amino acids that differ between the two sequences and changed to the mouse sequence for the individual chimeras are highlighted in red. Figure prepared using the GPCRdb database (www.gpcrdb.org).

the potency of Cl-IB-MECA to stimulate [^{35}S]GTPγS binding was similar (Supplemental Table 2). As shown in Fig. 3B and Supplemental Table 2, assays with the wild-type human A_3 AR LUF6000 increased the E_{max} of Cl-IB-MECA ~2.4-fold (Supplemental Table 2), demonstrating efficacy enhancement while decreasing its EC_{50} ~5-fold (from 19 to 90 nM). Our prior work indicates that the reduction in potency of Cl-IB-MECA produced by LUF6000 is due to competitive antagonism at the orthosteric binding site (Fisher et al., 2022). In contrast, LUF6000 failed to increase the E_{max} of Cl-IB-MECA in assays with the wild-type mouse A_3AR, although it continued to compete for binding at the orthosteric site, resulting in a reduction in the potency of Cl-IB-MECA (from 1 to 5 nM).

Assays using isolated HEK293 cell membranes expressing H/$M_{TMD3\text{-}4/ICL2}$ and H/$M_{TMD5\text{-}6/ICL3}$ chimeras determined susceptibility to efficacy enhancement by LUF6000 similar to that observed with wild-type human A_3ARs (Fig. 3B; Supplemental Table 2). Mild efficacy enhancement (~79% increase in the E_{max} of Cl-IB-MECA at a concentration of 10 μM versus vehicle) was observed in assays using H/$M_{TMD1\text{-}2/ICL1}$ membranes. Strikingly, however, when using H/$M_{TMD7/H8/CT}$ membranes LUF6000 failed to produce efficacy enhancement although it produced a substantial reduction in potency [EC_{50} of C-IB-MECA = 19 nM (vehicle) versus 966 nM (10 μM LUF6000)]. The loss in allosteric activity of LUF6000 unmasked its full antagonistic propensity (competition for orthosteric ligand binding), resulting in a dramatic rightward shift in the Cl-IB-MECA concentration-response curve. [^{125}I]I-AB-MECA (agonist) radioligand dissociation binding assays, which detect the pure allosteric actions of LUF6000 uncomplicated by its orthosteric effects, corroborated findings from the G protein activation assays where LUF6000 at a concentration of 10 μM was found to slow the rate of [^{125}I]I-AB-MECA dissociation in assays with the H/$M_{TMD1\text{-}2/ICL1}$, H/$M_{TMD3\text{-}4/ICL2}$, and H/$M_{TMD5\text{-}6/ICL3}$ chimeras (Fig. 3C, Supplemental Table 2). However, with the H/$M_{TMD7/H8/CT}$ chimera, LUF6000 no longer slowed [^{125}I]I-AB-MECA dissociation, indicating a loss of allosteric activity. Collectively, these results narrow the LUF6000 binding site to a region comprising the distal portions of TMD7 and H8. Results of the [^{35}S]GTPγS binding assays also suggest potential interactions with TMD1 and/or intracellular loop 1. TMD2 was ruled out since there are no amino acid differences in the lower portion of TMD2 between the human and mouse.

Molecular Modeling

To map the LUF6000 binding site, we created a structural model of the A_3AR using the AlphaFold multistate protocol (Heo and Feig, 2022). This is a modified version of AlphaFold (Jumper et al., 2021), which utilizes an annotated database of experimentally solved GPCR structures categorized according to their activation state. In this case, we modeled the human A_3AR in its active conformation. Subsequently, docking was performed with LUF6000 using the standard precision protocol of the Glide program (Friesner et al., 2004). Considering the results of the chimeric receptor studies, the predicted topology of the receptor's H8 region, and the hydrophobic properties of LUF6000, an extrahelical binding site was anticipated. Accordingly, the SiteMap tool (Halgren, 2007, 2009) was employed to search for hypothetical binding sites on the receptor surface (Supplemental Fig. 1), and the fourth-ranked site (site S4; SScore: 0.891, DScore 0.952) was found to be located at the interface among TMD1, TMD7, and H8, correlating precisely with the results of the human/mouse chimeric receptor studies. Thus, docking analysis with LUF6000 was concentrated on this region. Interestingly, four additional potential binding sites were identified from the SiteMap analysis in regions that are not consistent with the human/mouse chimeric receptor results (Supplemental Fig. 1). The top-ranked predicted binding site correlates with the putative orthosteric ligand binding site.

To generate possible LUF6000 binding poses within the S4 allosteric pocket, we carried out molecular docking analyses with the Glide program (Friesner et al., 2004), and calculations of the top five-ranked poses are provided in Supplemental Fig. 2. Because four of the poses (P1, P2, P3, and P5) were degenerate, the top-ranked P1 pose was selected as the putative LUF6000 binding mode, as depicted in Fig. 4. According to the model, the nearly planar 1*H*-imidazo[4,5-c]quinolin-4-amine ring system of LUF6000 lies parallel to the transmembrane segments, inserted into an aromatic pocket formed by Y284$^{7.55}$, F289$^{8.50}$,

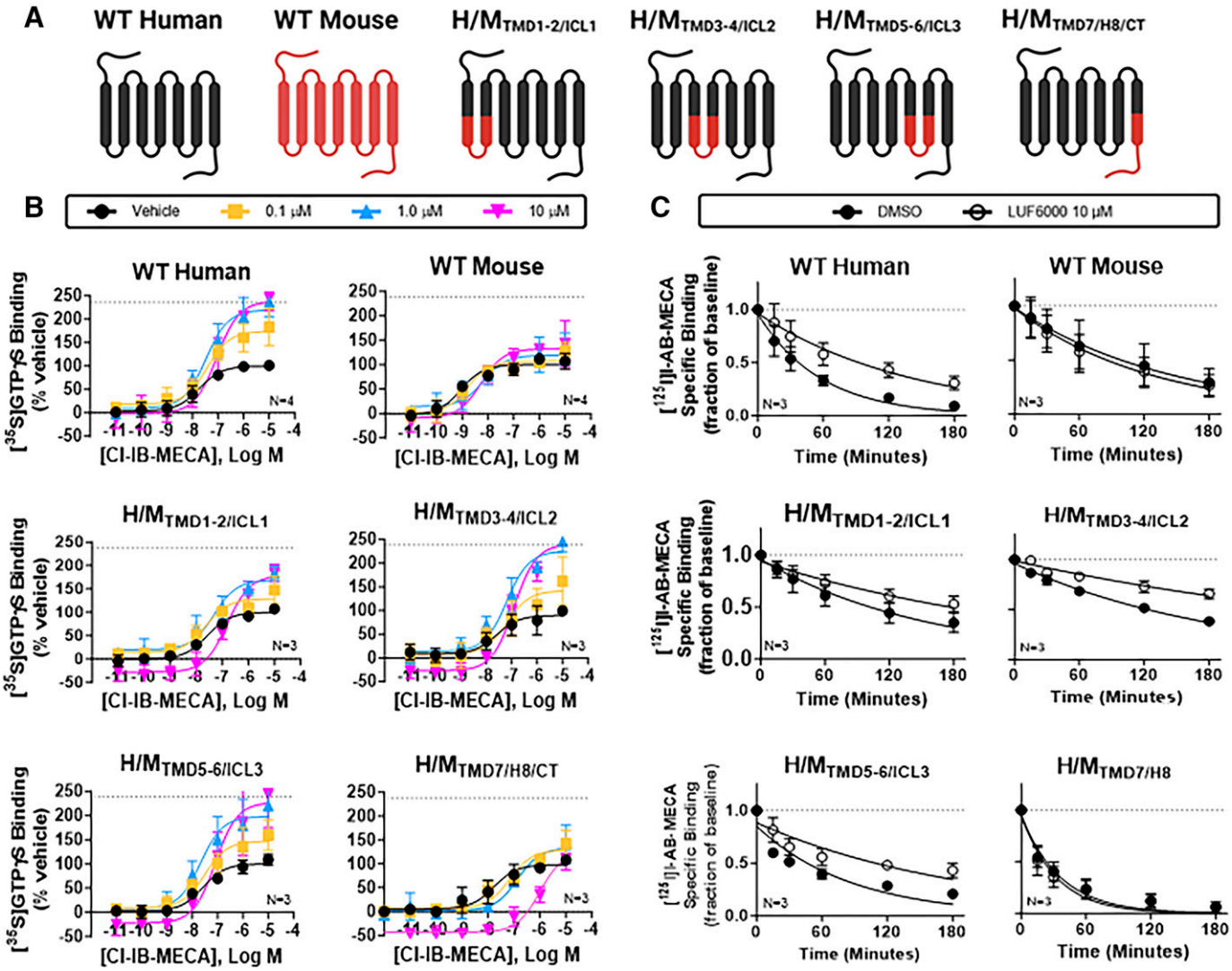

Fig. 3. Characterization of human/mouse chimeric A_3ARs. (A) Cartoon depicting the makeup of each chimeric receptor. (B) [^{35}S]GTPγS binding assays. Concentration-response curves with Cl-IB-MECA were conducted in the presence of vehicle (DMSO, black) or 0.1 (yellow), 1 (blue), or 10 μM (magenta) LUF6000. Results were normalized to the E_{max} value of Cl-IB-MECA obtained in the presence of vehicle. The dotted line in each graph demarcates the E_{max} of Cl-IB-MECA in the presence of 10 μM LUF6000 with membranes from wild-type A_3ARs (240 ± 11% of vehicle). (C) [^{125}I]I-AB-MECA dissociation binding assays. The allosteric actions of LUF6000 were lost in assays with the H/$M_{TMD7/H8/CT}$ chimera and diminished in assays with the H/$M_{TMD1-2/ICL1}$ chimera. EC_{50}, E_{max}, and k values are reported in Supplemental Table 2. Data are presented as the mean ± S.D.

and Y293$^{8.54}$. The 2-cyclohexyl group is positioned "upward" within a small hydrophobic subpocket (S4') created by residues M276$^{7.47}$, M277$^{7.48}$, P279$^{7.50}$, C25$^{1.45}$, V$^{1.48}$, and G29$^{1.49}$, while the 3,4-dichlorophenyl group extends toward the lipid interface via a π-π stacking interaction with the aromatic sidechain of Y284$^{7.55}$. Notably, no stabilizing H-bond interactions between LUF6000 and residues within the binding pocket were predicted. This was surprising considering the proximity of several highly interactive residues, notably Y284$^{7.55}$ and Y293$^{8.54}$. Thus, the pose suggests weak binding interactions. Because of the lack of H-bonding with the representative P1 pose, we investigated the merits of pose P4 (Supplemental Fig. 3), which is similar except the orientation of the heterocyclic scaffold is flipped such that the 3,4-dichlorophenyl group associates with the hydrophobic subpocket and the 2-cyclohexyl group extends toward the lipid interface without a π-π stacking interaction. Similarly, with this pose no H-bonding was predicted.

To further refine pose P1, multiple independent MD simulations were performed to reveal whether additional stabilizing interactions may form in a dynamic environment. Since the active-state conformation of GPCRs can rapidly devolve if left unrestrained (Latorraca et al., 2017), simulations were performed with the AlphaFold multistate A_3AR model complexed with a homology model of the $G\alpha_i$ subunit, based on the active-state cryo-electron microscopy structure of the A_1 AR bound to adenosine and complexed with the $G\alpha_{i2}$ subunit as a template (PDB ID: 7LD4; Draper-Joyce et al., 2021). In addition, C303$^{8.64}$ in H8 was palmitoylated due to its proximity to the putative LUF6000 binding site. Simulations were conducted identically either without (apo) or with (holo) LUF6000 bound to the S4 allosteric site, where the systems were 1) embedded within a phosphatidylcholine bilayer solvated with explicit water molecules containing a physiologic concentration of sodium chloride, 2) equilibrated for 40 ns, and 3) subjected to three independent MD replicates of 400 ns

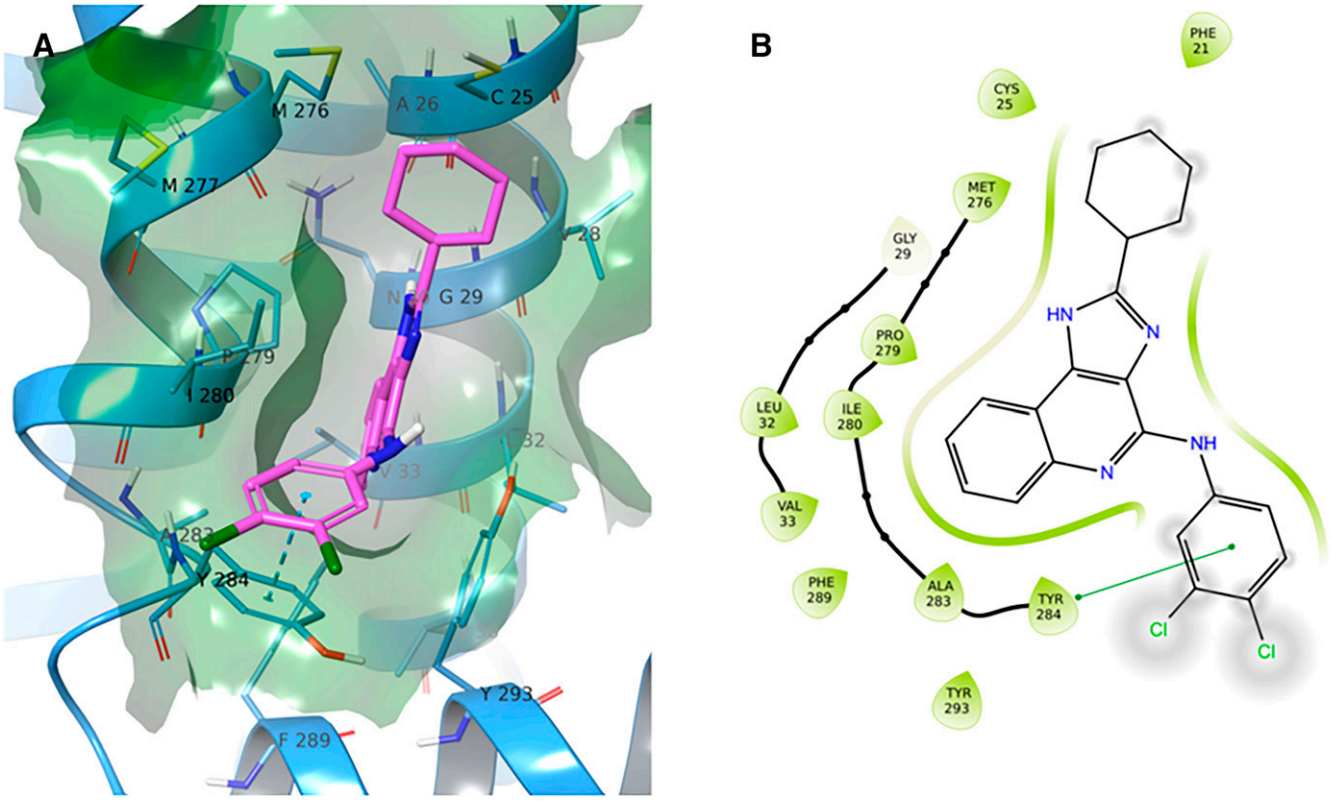

Fig. 4. Docking of LUF6000 with the AlphaFold model of the A_3AR. The top ranked pose (P1) for LUF6000 within the S4 allosteric site is shown. Panel A reports a three-dimensional representation of the pose, where LUF6000 is depicted in green and surrounding receptor residues within a 5 Å radius are shown in cornflower blue. Connolly surface is projected and colored according to the residue type coloring scheme of Maestro. Panel B illustrates the bidimensional interaction scheme for LUF6000 within the S4 pocket as provided by Maestro. A π-π stacking interaction is shown between Y284$^{7.55}$ and the 3,4-dichlorophenyl group of LUF6000. The 2-cyclohexyl group is positioned within a hydrophobic subpocket formed by residues in TMDs 1 and 7.

duration. Trajectories from the independent simulations were clustered based on the pairwise root mean square deviation (RMSD) matrix of the receptor backbone (apo system) or LUF6000 coordinates (holo system) with the TTCLUST Python package (Tubiana et al., 2018). For each cluster, the population size, expressed as a percentage of trajectory frames within the cluster, is reported.

MD Simulations with the Apo System. Cluster analyses of the apo system revealed an equilibrium between an open conformation of the binding site and a closed conformation, depending on the relative orientation of Y284$^{7.55}$ (Supplemental Fig. 4). In the closed conformation, Y284$^{7.55}$ stacks against Y293$^{8.54}$ and H-bonds with the backbone carbonyl of G29$^{1.49}$, completely closing the pocket and transforming it into a flat hydrophobic surface. In contrast, Y284$^{7.55}$ projects away from Y293$^{8.54}$ in the open conformation, allowing access to the pocket. The presence of an equilibrium between these two alternate conformations lends support to the proposed P1 docking pose, whereby components of LUF6000 may interact with Y284$^{7.55}$ and Y293$^{8.54}$ in the open conformation. Switching between the open and closed conformations can be observed in Supplemental Video 1, which reports a superposition between the three apo MD trajectories.

MD Simulations with the Holo System. Simulations performed on the holo system revealed instability of the P1 pose over long simulation times (see Supplemental Video 2 showing superposition of the three trajectories), as illustrated by both the ligand RMSD and interaction fingerprint similarity (Pavan et al., 2022) plots reported in Supplemental Fig. 5.

Specifically, in the first replicate (MD1) LUF6000 escapes the aromatic cage formed by Y284$^{7.55}$, F289$^{8.50}$, and Y293$^{8.54}$ to rearrange itself into a more membrane-exposed conformation stabilized by a direct H-bond between the exocyclic nitrogen and Y293$^{8.54}$, π-π stacking with Y293$^{8.54}$, and a water-bridged H-bond with the unpaired carbonyl of M276$^{7.47}$ and the N-1 nitrogen of the 1*H*-imidazo[4,5-c]quinolin-4-amine heterocycle (Supplemental Fig. 6, Supplemental Video 3). Notably, the presence of a water molecule in the small hydrophobic cleft between M276$^{7.47}$ and G25$^{1.45}$ was also observed in two high-resolution GPCR structures (5IU4 of an inactive-state A_{2A}AR in complex with ZM241385 and 5WIU of an inactive-state D_4 dopamine receptor in complex with nemonapride) used in the work of Venkatakrishnan and colleagues (Venkatakrishnan et al., 2019) to map conserved water molecules in GPCRs.

In the second replicate (MD2), which demonstrated the most stability based on its RMSD profile (Supplemental Fig. 5), LUF6000 maintains a conformation similar to the docking pose for most of the simulation but then eventually loses contact with Y293$^{8.54}$ (Supplemental Fig. 7, Supplemental Video 4). Although LUF6000 does not deviate from the starting position, the pocket does not stabilize, suggesting that the final position observed in this simulation represents a metastable intermediate rather than the bound state.

Finally, in the third simulation (MD3), LUF6000 transiently occupies the same metastable state observed at the end of the MD2 trial before rapidly converting to a different conformation that is maintained for the remainder of the trajectory (Fig. 5; Supplemental Video 5). Specifically, after ~50 ns, F289$^{8.50}$ flips away from its resting position and participates in π-π stacking with F48$^{2.40}$. This movement allows LUF6000 to insert deeper into the pocket, forming a stable H-bond (persistence = 21%) between the N-1 nitrogen of the 1*H*-imidazo[4,5-c]quinolin-4-amine heterocycle and the backbone carbonyl of G29$^{1.49}$. As a result, the heterocycle of LUF6000 forms a stabilizing π-π stacking interaction with Y293$^{8.54}$, whereas the exocyclic amine and the 3,4-dichlorophenyl group, respectively, form transient NH-π bonding and π-π stacking with Y284$^{7.55}$. In this position, the 2-cyclohexyl substituent is better accommodated into the hydrophobic S4' subpocket, forcing expulsion of the previously accommodated water molecule (Fig. 5; Supplemental Video 5).

Clustering analyses of the holo trials support claims derived from visual inspection of the individual trajectories (Supplemental Fig. 8). Specifically, clusters C1, C3, and C4 represent degenerate solutions loosely resembling the docking pose, with LUF6000 π-π stacking and forming a series of close-range hydrophobic interactions with residues surrounding the pocket. With each of these clusters, contact with Y293$^{8.54}$ is absent, resulting in positioning of the distal portion of H8 further away from the cytosolic ends of TMDs 7 and 1. Cluster C2, which is the most highly populated cluster and is predicted to represent the final bound state, closely resembles the final state of MD3, with LUF6000 deeply buried within the site S4 pocket, whereas cluster C5 resembles the final state observed in MD1, where LUF6000 becomes more membrane exposed. Interestingly, in both of these clusters, H8 is tilted "upwards" closer in space to TM7 and TM1, presumably as a result of LUF6000 functioning as a molecular glue upon establishment of additional interactions with Y293$^{8.54}$. Considering that Lu and colleagues (Lu et al., 2021) recently proposed that tilting of H8 is a requirement for the angiotensin-II receptor to become activated, cluster C2 provides an attractive explanation for LUF6000's pharmacological actions as a positive allosteric modulator. Moreover, it is reasonable to assume that the remaining clusters (C1/C3/C4 defined as metastate 1 and C5 defined as metastate 2) represent intermediate binding states that precede the bound state (cluster 2). To directly test this hypothesis, we extended the MD1 simulation for an additional 100 ns to determine whether the C5 conformation converts to a bound state. Strikingly, LUF6000 rapidly evolved toward a metastable state 1-like state before eventually converging to a C2-like bound conformation (Supplemental Video 6). This finding supports the idea that H-bonding and π-π stacking interactions with both Y284$^{7.55}$ and Y293$^{8.54}$ are pivotal in attracting and maneuvering LUF6000 into the S4 binding pocket.

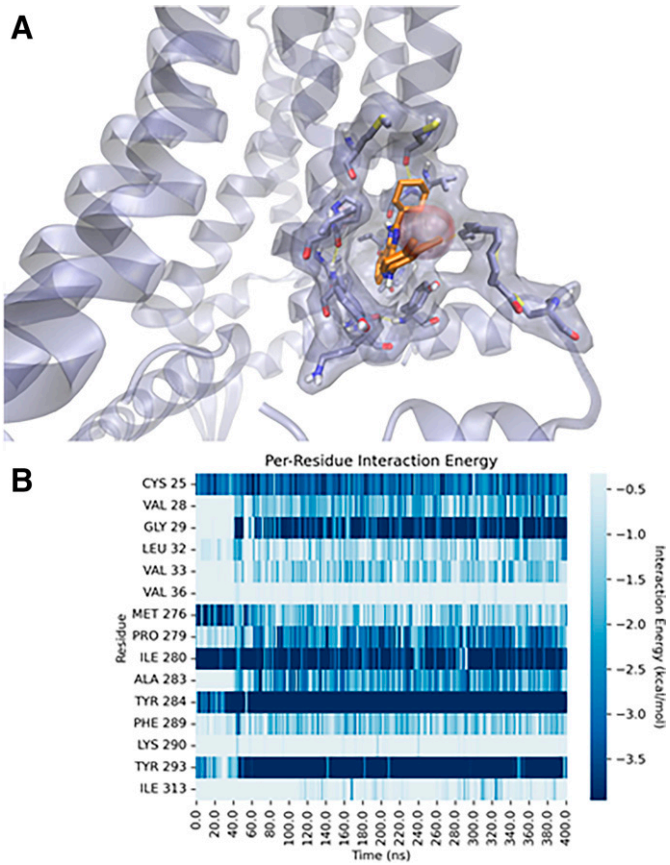

Fig. 5. Final state of the third molecular dynamics (MD3) refinement performed on the P1 docking pose proposed to represent the bound state of LUF6000 with the S4 site. Panel A shows a three-dimensional representation of the final state of the simulation. Panel B shows per-residue decomposition of the receptor-ligand interaction energy throughout the 400 ns simulation.

Additional Mutagenesis

The predicted binding mode was validated by mutagenesis experiments, wherein allosteric enhancing activity of LUF6000 was greatly reduced in [^{35}S]GTPγS exchange and [^{125}I]I-AB-MECA dissociation binding assays when Y284$^{7.55}$ was mutated to a cysteine correlating with the mouse sequence (Fig. 6; Supplemental Table 2). In addition, PAM activity of LUF6000 was lost entirely when Y293$^{8.54}$ was changed to phenylalanine (Fig. 6; Supplemental Table 2). However, with both tyrosine mutants, the orthosteric competitive nature of LUF6000 persisted. According to the model, the dramatic effect of the loss of a single oxygen atom in the Y293$^{8.54}$ mutation supports the hypothesis that the Y293$^{8.54}$ hydroxyl group participates in H-bonding with the exocyclic nitrogen of LUF6000 during transition to the final bound state.

The possibility of a specific H-bond between the exocyclic NH, acting as a donor, and Y293$^{8.54}$ was further strengthened by the observation that enhancing activity was reduced with LUF6000 derivatives in which the exocyclic nitrogen was replaced with other heteroatoms or methylated (Fig. 7; Supplemental Table 3). We synthesized analogs with ether, thioether, or methylamino substitutions in place of the exocyclic NH as described in the Supplemental Chemical Synthesis section in the Supplemental Material file; each of these analogs cannot donate a H-bond to the receptor protein. Correspondingly, we also synthesized ether and thioether derivatives of LUF6000 at position 1 of the heterocycle that lack the ability to donate an H-bond, which were also found to exhibit submaximal PAM activity (Fig. 8; Supplemental Table 3).

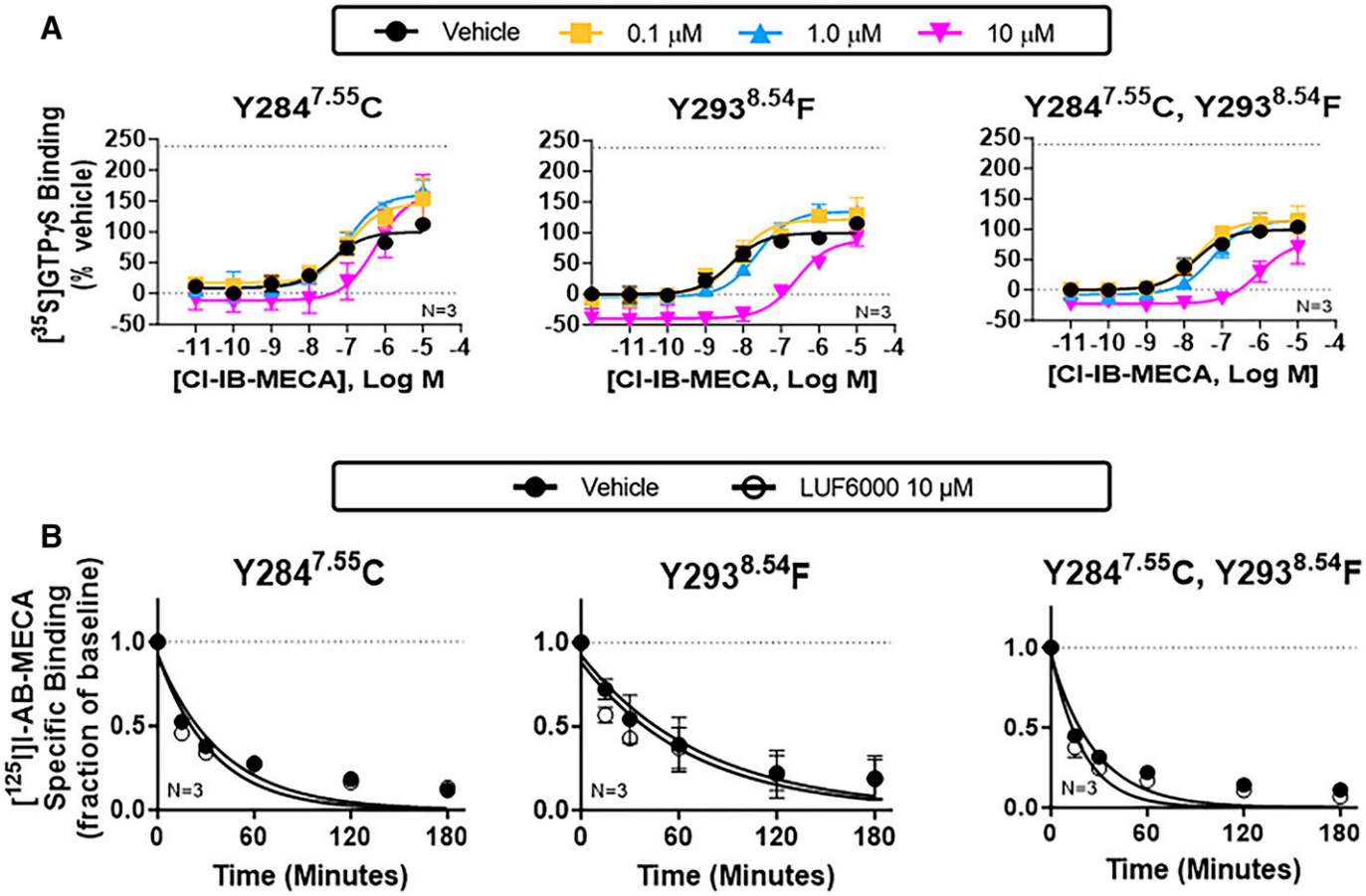

Fig. 6. Characterization of Y284$^{7.55}$C and Y293$^{8.54}$F mutant receptors. [^{35}S]GTPγS (A) and [^{125}I]I-AB-MECA dissociation (B) binding assays with HEK293 cell membranes expressing Y284$^{7.55}$C or Y293$^{8.54}$F mutant receptors alone or in combination. The allosteric actions of LUF6000 were lost with either mutation, supporting the participation of π-π stacking with Y284$^{7.55}$ and Y293$^{8.54}$ and H-bonding between Y293$^{8.54}$ and the exocyclic nitrogen of LUF6000 as critical interactions for LUF6000 binding to the proposed S4 allosteric site. For the [^{35}S]GTPγS binding assays, concentration-response curves with Cl-IB-MECA were conducted in the presence of vehicle (DMSO, black) or 0.1 (yellow), 1 (blue), or 10 μM (magenta) LUF6000. Results were normalized to the E_{max} value of Cl-IB-MECA obtained in the presence of vehicle. The dotted line in each graph demarcates the E_{max} of Cl-IB-MECA in the presence of 10 μM LUF6000 with membranes from wild-type A_3ARs (240 ± 11% of vehicle). EC_{50}, E_{max}, and k values are reported in Supplemental Table 2. Data are presented as the mean ± S.D.

Discussion

This study describes a putative binding region and molecular interactions for the prototypical 1*H*-imidazo[4,5-c]quinolin-4-amine allosteric modulator LUF6000. Molecular modeling, guided and further supported by mutagenesis and pharmacological studies, predicts that LUF6000 occupies an extrahelical, lipid-facing allosteric pocket formed by TMD1, TMD7, and H8. The putative binding region does not overlap with the orthosteric binding site, and no amino acid residues are shared between the two sites.

This putative binding mode is contrary to prior computational modeling predictions with the A_3AR (Gao et al., 2003; Deganutti et al., 2015) but is highly consistent with structure-activity-relationship information accumulated by our group with 1*H*-imidazo[4,5-c]quinolin-4-amine PAMs. For full PAM activity, hydrophobic substitutions are required at the 2- and 4-amine positions of the 1*H*-imidazo[4,5-c]quinolin-4-amine heterocycle, whereas polar substitutions are not tolerated (Gao et al., 2002; Göblyös et al., 2006; Kim et al., 2009; Fallot et al., 2022; Fisher et al., 2022). Concerning the 2-position, this requirement was demonstrated in comprehensive evaluation of 1*H*-imidazo[4,5-c]quinolin-4-amine derivatives with 2-cycloalkyl substitutions ranging from 3 to 12 carbons, wherein full PAM activity was achieved with 2-cyclohexyl or 2-cycloheptyl substitutions; activity progressively diminished with the addition of larger or smaller substitutions (Fisher et al., 2022). Additional work established that PAM activity is lost upon introducing nitrogen or oxygen to comparable ring systems at the 2-position to increase polarity (Fallot et al., 2022). However, less structure-activity-relationship work has focused on the 4-position. Nevertheless, we previously showed that an aryl substituent is greatly favored over heterocyclic ring systems with greater polarity (Göblyös et al., 2006; Kim et al., 2009).

Considering the extensive prior structure-activity-relationship work and the proposed binding pose of LUF6000 described in this study, we present the hypothesis that the 1*H*-imidazo[4,5-c]quinolin-4-amine ring system inserts into an aromatic cage formed by Y284$^{7.55}$ in TMD7 and Y293$^{8.54}$ in H8 (Figs. 4 and 5), which becomes accessible when Y284$^{7.55}$ positions to an open conformation. The 2-cyclohexyl group is situated within a hydrophobic subpocket created by residues in TMDs 1 and 7, while the 3,4-dichlorohexyl group extends toward the lipid bilayer, which due to its hydrophobic nature may provide additional stabilization. A_3AR-specificity in

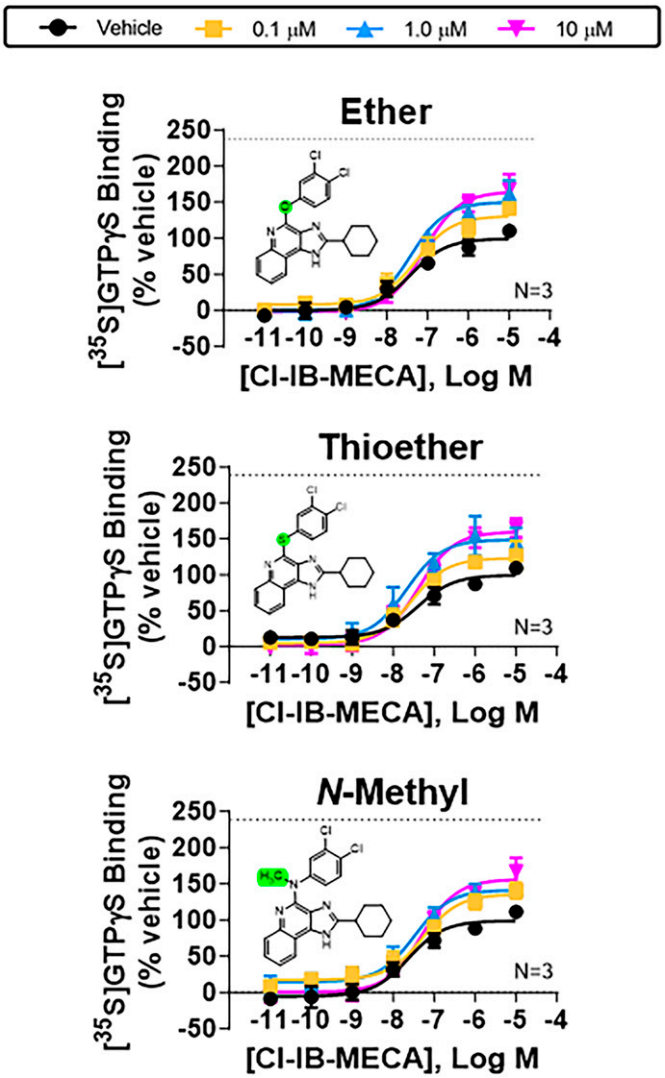

Fig. 7. Characterization of exocyclic ether, thioether, and N-methyl derivatives of LUF6000 with wild-type A_3ARs. [^{35}S]GTPγS binding assays assessing effects of increasing concentrations of the indicated exocyclic ether, thioether, or N-methyl derivatives of LUF6000 with HEK293 cell membranes expressing wild-type A_3ARs. Allosteric actions of all the derivatives were diminished compared with LUF6000, supporting the hypothesis for H-bonding between the exocyclic nitrogen of LUF6000 and the hydroxyl of Y293$^{8.54}$. Concentration-response curves with Cl-IB-MECA were conducted in the presence of vehicle (DMSO, black) or 0.1 (yellow), 1 (blue), or 10 μM (magenta) of the indicated derivatives. The dotted line in each graph demarcates the E_{max} of Cl-IB-MECA in the presence of 10 μM LUF6000 with membranes from wild-type A_3ARs (240 ± 11% of vehicle). EC_{50} and E_{max} values are reported in Supplemental Table 7. Data are presented as the mean ± S.D.

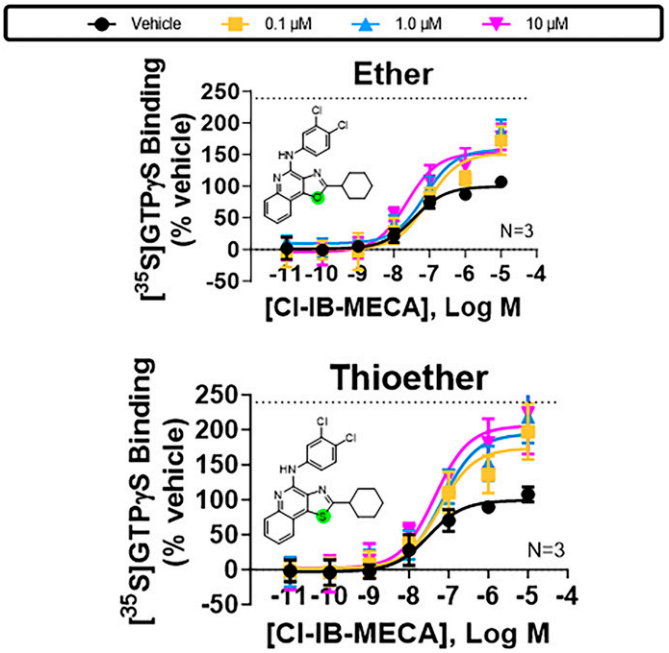

Fig. 8. Characterization of ether and thioether derivatives of LUF6000 at the N-1 position of the imidazole ring with wild-type A_3ARs. [^{35}S]GTPγS binding assays assessing effects of increasing concentrations of the indicated ether and thioether derivatives of LUF6000 with HEK293 cell membranes expressing wild-type A_3ARs. Allosteric actions of both derivatives were diminished as compared with LUF6000, supporting the hypothesis for H-bonding between the N-1 nitrogen of the heterocycle of LUF6000 and the hydroxyl of Y293$^{8.54}$. Concentration-response curves with Cl-IB-MECA were conducted in the presence of vehicle (DMSO, black) or 0.1 (yellow), 1 (blue), or 10 μM (magenta) of the derivatives. The dotted line in each graph demarcates the E_{max} of Cl-IB-MECA in the presence of 10 μM LUF6000 with membranes from wild-type A_3ARs (240 ± 11% of vehicle). EC_{50} and E_{max} values are reported in Supplemental Table 7. Data are presented as mean ± S.D.

relation to the other adenosine receptor subtypes, demonstrated in prior published work (Fallot et al., 2022), is explained by replacing the critical Y293$^{8.54}$ with phenylalanine, whereas nonresponsiveness of the mouse A_3AR to LUF6000 is explained by replacing the critical Y284$^{7.55}$ with a cysteine. Based on the chimeric receptor studies, we exchanged the entire distal portions of the mouse A_3AR sequence with the human sequence, which included the distal half of TMD7, H8, and the C-terminus. However, responsiveness to LUF6000 was not conferred with the newly created chimeric receptors in [^{35}S]GTPγS exchange assays (Supplemental Fig. 9, Supplemental Table 2). Thus, amino acid differences in other regions of the receptor, presumably TMD1 based on the previous chimeric receptor and modeling results, also appear to contribute to species differences.

In a prior mutagenesis study conducted by our group 20 years ago when the structural assessment of GPCRs was in its infancy (Gao et al., 2003), we explored the participation of several amino acid residues in mediating the allosteric actions of three structurally dissimilar PAMs. DU124183, a 1*H*-imidazo[4,5-c]quinolin-4-amine derivative that contains 2-cyclopentyl and 4-aminophenyl substituents (Supplemental Fig. 10), was included in this investigation. We reported that the allosteric actions of DU124183, detected by slowed [^{125}I]I-AB-MECA dissociation, were reduced with each of the following mutants: N30A$^{1.50}$, D58N$^{2.50}$, D107N$^{3.49}$, F182A$^{5.43}$, and N274A$^{7.45}$ (Gao et al., 2003). Considering that within the family of adenosine receptors it is now known that each of these residues are required for receptor rearrangement, sodium binding, or orthosteric ligand binding, loss of activity of DU124183 with each of these mutations is predicted to affect the receptor's ability to transition between active and inactive states or affect cooperative interactions between the orthosteric and allosteric sites rather than the ability of DU124183 to bind to its allosteric site. Notably, the mutant receptors in this original study were not investigated in assays to assess G protein activation, and each of the amino acids is conserved among the human and mouse sequences (conserved in all species where the A_3AR sequence has been reported).

At this time, we can only speculate on the molecular mechanism of LUF6000s allosteric effects. As described with other

PAMs (Burger et al., 2018; Wang et al., 2018; Liu et al., 2019; van der Westhuizen et al., 2021; Nguyen et al., 2022), LUF6000 may favorably alter the conformational equilibrium of the receptor toward an active compared with the inactive state. Regarding the antagonistic nature of LUF6000 that occurs at concentrations approaching 10 μM, we have previously found this to be consistent with competitive inhibition at the orthosteric binding site rather than negative allosterism (Fallot et al., 2022; Fisher et al., 2022). This was confirmed using "inner" and "outer" (with respect to the plasma membrane) human/mouse chimeric receptors, where the positive allosteric activity of LUF6000 was lost when the inner portions of the receptor were comprised of the mouse sequence, yet its competitive antagonistic actions persisted (Fisher et al., 2022). This conclusion was further supported by studies with the antagonist radioligand ^{125}I-ABOPX, where LUF6000 was found to reduce specific binding to zero in equilibrium binding assays, and by docking studies with a homology model of the A_3AR where LUF6000 could be accommodated into the canonical AR orthosteric binding site as we described (Fallot et al., 2022; Fisher et al., 2022).

The allosteric site described herein correlates closely with orphan site 9 (OS9) predicted through a computational study aimed to define the GPCR "pocketome" (Hedderich et al., 2022). Through exhaustive docking analysis of a library of small molecule probes with structures from 113 unique receptors (557 unique structures), this study confirmed all previously identified allosteric pockets and revealed 9 untargeted sites termed orphan sites. Like the proposed LUF6000 binding site we have described, OS9 is an exofacial site that lies between TMDs 1 and 7 above H8. In a computational study aimed to describe activation mechanisms of the angiotensin type II receptor, Lu and colleagues (Lu et al., 2021) identified a "cryptic" binding pocket similar to OS9, which was termed pocket P6. Via mutational analysis of representative receptors (angiotensin II, M_3 muscarinic, and β_2 adrenergic), both of these studies provided evidence that amino acids surrounding this site have a robust effect on both G protein activation and β-arrestin recruitment, suggesting the modulatory potential of ligands that occupy this site (Lu et al., 2021; Hedderich et al., 2022). The position and shape of the OS9 pocket was predicted to be highly conserved and was proposed to be a pan-class A GPCR pocket.

In conclusion, here we have provided computational, mutagenesis, and pharmacological evidence supporting an extrahelical binding site for the 1*H*-imidazo[4,5-c]quinolin-4-amine A_3 AR PAM LUF6000. This site is likely shared among other GPCRs based on past computational predictions of potential allosteric sites for the broad family of GPCRs. This study has provided new structural insights for the A_3AR and will aid rational approaches to design improved allosteric ligands.

Data Availability

The authors declare that all the data supporting the findings of this study are available within the paper and Supplemental Material. A PDB structure reporting the heavy atom coordinates of the human A_3AR model bound to LUF6000 (obtained through InducedFit Docking) is in a separate Supplemental Material file.

Authorship Contributions

Participated in research design: Fisher, Pavan, Salmaso, Keyes, Wan, Pradhan, Gao, Smith, Jacobson, Auchampach.

Conducted experiments: Fisher, Pavan, Salmaso, Keyes, Wan, Auchampach.

Contributed new reagents: Keyes, Pradhan, Smith, Jacobson.

Performed data analysis: Fisher, Pavan, Salmaso, Keyes, Wan, Auchampach.

Wrote or contributed to the writing of the manuscript: Fisher, Pavan, Jacobson, Auchampach.

References

Antonioli L, Pacher P, and Haskó G (2022) Adenosine and inflammation: it's time to (re)solve the problem. *Trends Pharmacol Sci* **43:**43–55.

Auchampach JA, Jin X, Wan TC, Caughey GH, and Linden J (1997) Canine mast cell adenosine receptors: cloning and expression of the A3 receptor and evidence that degranulation is mediated by the A2B receptor. *Mol Pharmacol* **52:**846–860.

Ballesteros JA and Weinstein H (1995) Integrated methods for the construction of three-dimensional models and computational probing of structure-function relations in G protein-coupled receptors. *Methods in Neirosciences* **25:**366–428.

Bozdemir E, Vigil FA, Chun SH, Espinoza L, Bugay V, Khoury SM, Holstein DM, Stoja A, Lozano D, Tunca C et al. (2021) Neuroprotective roles of the adenosine A_3 receptor agonist AST-004 in mouse model of traumatic brain injury. *Neurotherapeutics* **18:**2707–2721.

Burger WAC, Sexton PM, Christopoulos A, and Thal DM (2018) Toward an understanding of the structural basis of allostery in muscarinic acetylcholine receptors. *J Gen Physiol* **150:**1360–1372.

Chen Y, Corriden R, Inoue Y, Yip L, Hashiguchi N, Zinkernagel A, Nizet V, Insel PA, and Junger WG (2006) ATP release guides neutrophil chemotaxis via P2Y2 and A3 receptors. *Science* **314:**1792–1795.

Coughlin Q, Hopper AT, Blanco MJ, Tirunagaru V, Robichaud AJ, and Doller D (2019) Allosteric modalities for membrane-bound receptors: insights from drug hunting for brain diseases. *J Med Chem* **62:**5979–6002.

Deganutti G, Cuzzolin A, Ciancetta A, and Moro S (2015) Understanding allosteric interactions in G protein-coupled receptors using supervised molecular dynamics: a prototype study analysing the human A3 adenosine receptor positive allosteric modulator LUF6000. *Bioorg Med Chem* **23:**4065–4071.

Draper-Joyce CJ, Bhola R, Wang J, Bhattarai A, Nguyen ATN, Cowie-Kent I, O'Sullivan K, Chia LY, Venugopal H, Valant C et al. (2021) Positive allosteric mechanisms of adenosine A_1 receptor-mediated analgesia. *Nature* **597:**571–576.

Du L, Gao ZG, Nithipatikom K, IJzerman AP, Veldhoven JP, Jacobson KA, Gross GJ, and Auchampach JA (2012) Protection from myocardial ischemia/reperfusion injury by a positive allosteric modulator of the A_3 adenosine receptor. *J Pharmacol Exp Ther* **340:**210–217.

Du L, Gao ZG, Paoletta S, Wan TC, Gizewski ET, Barbour S, van Veldhoven JPD, IJzerman AP, Jacobson KA, and Auchampach JA (2018) Species differences and mechanism of action of A_3 adenosine receptor allosteric modulators. *Purinergic Signal* **14:**59–71.

Fallot LB, Suresh RR, Fisher CL, Salmaso V, O'Connor RD, Kaufman N, Gao ZG, Auchampach JA, and Jacobson KA (2022) Structure-activity studies of 1*H*-imidazo[4,5-*c*]quinolin-4-amine derivatives as A_3 adenosine receptor positive allosteric modulators. *J Med Chem* **65:**15238–15262.

Fisher CL, Fallot LB, Wan TC, Keyes RF, Suresh RR, Rothwell AC, Gao ZG, McCorvy JD, Smith BC, Jacobson KA et al. (2022) Characterization of dual-acting A_3 adenosine receptor positive allosteric modulators that preferentially enhance adenosine-induced $G\alpha_{i3}$ and $G\alpha_{oA}$ isoprotein activation. *ACS Pharmacol Transl Sci* **5:**625–641.

Fishman P, Stemmer SM, Bareket-Samish A, Silverman MH, and Kerns WD (2023) Targeting the A3 adenosine receptor to treat hepatocellular carcinoma: anti-cancer and hepatoprotective effects. *Purinergic Signal* **19:**513–522.

Friesner RA, Banks JL, Murphy RB, Halgren TA, Klicic JJ, Mainz DT, Repasky MP, Knoll EH, Shelley M, Perry JK et al. (2004) Glide: a new approach for rapid, accurate docking and scoring. 1. Method and assessment of docking accuracy. *J Med Chem* **47:**1739–1749.

Gao ZG, Auchampach JA, and Jacobson KA (2023) Species dependence of A(3) adenosine receptor pharmacology and function. *Purinergic Signal* **19:**523–550.

Gao ZG, Kim SG, Soltysiak KA, Melman N, IJzerman AP, and Jacobson KA (2002) Selective allosteric enhancement of agonist binding and function at human A3 adenosine receptors by a series of imidazoquinoline derivatives. *Mol Pharmacol* **62:**81–89.

Gao ZG, Kim SK, Gross AS, Chen A, Blaustein JB, and Jacobson KA (2003) Identification of essential residues involved in the allosteric modulation of the human A(3) adenosine receptor. *Mol Pharmacol* **63:**1021–1031.

Gao ZG, Verzijl D, Zweemer A, Ye K, Göblyös A, IJzerman AP, and Jacobson KA (2011) Functionally biased modulation of A(3) adenosine receptor agonist efficacy and potency by imidazoquinolinamine allosteric enhancers. *Biochem Pharmacol* **82:**658–668.

Gao ZG, Ye K, Göblyös A, IJzerman AP, and Jacobson KA (2008) Flexible modulation of agonist efficacy at the human A3 adenosine receptor by the imidazoquinoline allosteric enhancer LUF6000. *BMC Pharmacol* **8:**20.

Ge ZD, van der Hoeven D, Maas JE, Wan TC, and Auchampach JA (2010) A(3) adenosine receptor activation during reperfusion reduces infarct size through actions on bone marrow-derived cells. *J Mol Cell Cardiol* **49:**280–286.

Göblyös A, Gao ZG, Brussee J, Connestari R, Santiago SN, Ye K, IJzerman AP, and Jacobson KA (2006) Structure-activity relationships of new 1H-imidazo[4,5-c]quinolin-4-amine derivatives as allosteric enhancers of the A3 adenosine receptor. *J Med Chem* **49:**3354–3361.

Halgren T (2007) New method for fast and accurate binding-site identification and analysis. *Chem Biol Drug Des* **69:**146–148.

Halgren TA (2009) Identifying and characterizing binding sites and assessing druggability. *J Chem Inf Model* **49:**377–389.

Hammarberg C, Schulte G, and Fredholm BB (2003) Evidence for functional adenosine A3 receptors in microglia cells. *J Neurochem* **86:**1051–1054.

Haskó G, Linden J, Cronstein B, and Pacher P (2008) Adenosine receptors: therapeutic aspects for inflammatory and immune diseases. *Nat Rev Drug Discov* **7:**759–770.

Hedderich JB, Persechino M, Becker K, Heydenreich FM, Gutermuth T, Bouvier M, Bünemann M, and Kolb P (2022) The pocketome of G-protein-coupled receptors reveals previously untargeted allosteric sites. *Nat Commun* **13:**2567.

Heo L and Feig M (2022) Multi-state modeling of G-protein coupled receptors at experimental accuracy. *Proteins* **90:**1873–1885.

Jordan JE, Thourani VH, Auchampach JA, Robinson JA, Wang NP, and Vinten-Johansen J (1999) A(3) adenosine receptor activation attenuates neutrophil function and neutrophil-mediated reperfusion injury. *Am J Physiol* **277:**H1895–H1905.

Jumper J, Evans R, Pritzel A, Green T, Figurnov M, Ronneberger O, Tunyasuvunakool K, Bates R, Žídek A, Potapenko A et al. (2021) Highly accurate protein structure prediction with AlphaFold. *Nature* **596:**583–589.

Kim Y, de Castro S, Gao ZG, IJzerman AP, and Jacobson KA (2009) Novel 2- and 4-substituted 1H-imidazo[4,5-c]quinolin-4-amine derivatives as allosteric modulators of the A3 adenosine receptor. *J Med Chem* **52:**2098–2108.

Latorraca NR, Venkatakrishnan AJ, and Dror RO (2017) GPCR dynamics: structures in motion. *Chem Rev* **117:**139–155.

Liston TE, Hama A, Boltze J, Poe RB, Natsume T, Hayashi I, Takamatsu H, Korinek WS, and Lechleiter JD (2022) Adenosine A1R/A3R (adenosine A1 and A3 receptor) agonist AST-004 reduces brain infarction in a nonhuman primate model of stroke. *Stroke* **53:**238–248.

Liston TE, Hinz S, Müller CE, Holstein DM, Wendling J, Melton RJ, Campbell M, Korinek WS, Suresh RR, Sethre-Hofstad DA et al. (2020) Nucleotide $P2Y_1$ receptor agonists are in vitro and in vivo prodrugs of A_1/A_3 adenosine receptor agonists: implications for roles of $P2Y_1$ and A_1/A_3 receptors in physiology and pathology. *Purinergic Signal* **16:**543–559.

Liu X, Masoudi A, Kahsai AW, Huang LY, Pani B, Staus DP, Shim PJ, Hirata K, Simhal RK, Schwalb AM et al. (2019) Mechanism of β_2AR regulation by an intracellular positive allosteric modulator. *Science* **364:**1283–1287.

Lu S, He X, Yang Z, Chai Z, Zhou S, Wang J, Rehman AU, Ni D, Pu J, Sun J et al. (2021) Activation pathway of a G protein-coupled receptor uncovers conformational intermediates as targets for allosteric drug design. *Nat Commun* **12:**4721.

Melman A, Gao ZG, Kumar D, Wan TC, Gizewski E, Auchampach JA, and Jacobson KA (2008) Design of (N)-methanocarba adenosine 5′-uronamides as species-independent A3 receptor-selective agonists. *Bioorg Med Chem Lett* **18:**2813–2819.

Nguyen HTM, van der Westhuizen ET, Langmead CJ, Tobin AB, Sexton PM, Christopoulos A and Valant C (2022) Opportunities and challenges for the development of M(1) muscarinic receptor positive allosteric modulators in the treatment for neurocognitive deficits. *Br J Pharmacol,* in press.

Paoletta S, Tosh DK, Finley A, Gizewski ET, Moss SM, Gao ZG, Auchampach JA, Salvemini D, and Jacobson KA (2013) Rational design of sulfonated A3 adenosine receptor-selective nucleosides as pharmacological tools to study chronic neuropathic pain. *J Med Chem* **56:**5949–5963.

Pavan M, Menin S, Bassani D, Sturlese M, and Moro S (2022) Implementing a scoring function based on interaction fingerprint for Autogrow4: protein kinase CK1δ as a case study. *Front Mol Biosci* **9:**909499.

Slosky LM, Caron MG, and Barak LS (2021) Biased allosteric modulators: new frontiers in GPCR drug discovery. *Trends Pharmacol Sci* **42:**283–299.

Tubiana T, Carvaillo JC, Boulard Y, and Bressanelli S (2018) TTClust: a versatile molecular simulation trajectory clustering program with graphical summaries. *J Chem Inf Model* **58:**2178–2182.

van der Hoeven D, Gizewski ET, and Auchampach JA (2010) Activation of the A(3) adenosine receptor inhibits fMLP-induced Rac activation in mouse bone marrow neutrophils. *Biochem Pharmacol* **79:**1667–1673.

van der Hoeven D, Wan TC, and Auchampach JA (2008) Activation of the A(3) adenosine receptor suppresses superoxide production and chemotaxis of mouse bone marrow neutrophils. *Mol Pharmacol* **74:**685–696.

van der Westhuizen ET, Choy KHC, Valant C, McKenzie-Nickson S, Bradley SJ, Tobin AB, Sexton PM, and Christopoulos A (2021) Fine tuning muscarinic acetylcholine receptor signaling through allostery and bias. *Front Pharmacol* **11:**606656.

Venkatakrishnan AJ, Ma AK, Fonseca R, Latorraca NR, Kelly B, Betz RM, Asawa C, Kobilka BK, and Dror RO (2019) Diverse GPCRs exhibit conserved water networks for stabilization and activation. *Proc Natl Acad Sci USA* **116:**3288–3293.

Walker BA, Jacobson MA, Knight DA, Salvatore CA, Weir T, Zhou D, and Bai TR (1997) Adenosine A3 receptor expression and function in eosinophils. *Am J Respir Cell Mol Biol* **16:**531–537.

Wang X, Heinz BA, Qian YW, Carter JH, Gadski RA, Beavers LS, Little SP, Yang CR, Beck JP, Hao J et al. (2018) Intracellular binding site for a positive allosteric modulator of the dopamine D1 receptor. *Mol Pharmacol* **94:**1232–1245.

Wang Y, Yu Z, Xiao W, Lu S, and Zhang J (2021) Allosteric binding sites at the receptor-lipid bilayer interface: novel targets for GPCR drug discovery. *Drug Discov Today* **26:**690–703.

Address correspondence to: Dr. John A. Auchampach, 8701 Watertown Plank Road, Milwaukee, WI 53226. E-mail: jauchamp@mcw.edu; or Dr. Kenneth A. Jacobson, Building 8A, Room B1A-19, 9000 Rockville Pike, Bethesda, MD 20892. E-mail: kennethj@niddk.nih.gov